Clays and Clay Minerals, Vol. 51, No. 5, 570–576, 2003.

DISORDER IN LAYERED HYDROXIDES: DIFFaX SIMULATION OF THE X-RAY POWDER DIFFRACTION PATTERNS OF NICKEL HYDROXIDE

T. N. Ramesh, R. S. Jayashree and P. Vishnu Kamath*

Department of Chemistry, Central College, Bangalore University, Bangalore 560 001, India

Abstract—Layered metal hydroxides exhibit non-uniform broadening of lines in their X-ray powder diffraction (XRPD) patterns, which cannot always be explained on the basis of crystallite size effects. In the case of hexagonal solids such as nickel hydroxide, DIFFaX simulations of the XRPD patterns show that: (1) stacking faults and turbostratic disorder at low (<30%) incidence selectively broaden the *h*0*l* reflections; (2) turbostratic disorder at high (>40%) incidence causes asymmetric broadening of the *hk*0 reflections and a complete extinction of the *hkl* reflections while leaving 00*l* unchanged; (3) interstratification selectively broadens the non-*hk*0 reflections; and (4) cation vacancies reduce the relative intensity of the 100 reflection. In contrast, a reduction in the thickness of the crystallites along the stacking direction of the layers selectively broadens the 00*l* reflections while a reduction in the disc diameter causes the progressive broadening and extinction of the *hk*0 reflections. Comparison with experimental data shows that several kinds of disorders have to be invoked to account for the observed broadening. DIFFaX simulations enable the quantification of the different kinds of disorder.

Key Words—Cation Vacancies, Crystallite Size, DIFFaX, Interstratification, Nickel Hydroxide, Stacking Faults, Turbostraticity.

INTRODUCTION

The interaction of X-rays with the powdered form of a crystalline solid results in sharp Bragg reflections whose positions and relative intensities are characteristic of the structure of the solid. Often, however, the peaks corresponding to different reflections in the XRPD pattern are broadened considerably. The broadening of peaks is generally ascribed to particle-size effects (West, 1987). In many instances, the broadening of peaks is non-uniform. By applying the Scherrer formula to each of the reflections individually, many authors have estimated the particle size in each crystallographic direction separately (Bernard *et al*., 1996). But difficulties with this approach arise when: (1) the broadening is non-uniform and is characteristic of certain families of planes; (2) the broadening is so excessive as to yield unrealistically small crystallite size; and (3) relative intensities of different reflections vary from one preparation to another, even when the solid is known to crystallize in a particular structure.

In such situations, it becomes imperative to look for causes other than crystallite size to explain the broadening of Bragg peaks in the XRPD patterns. One of the most obvious causes is the loss of crystallinity due to incorporation of various kinds of disorder during crystallization. This is particularly true of layered solids such as clays. The subject matter of 'crystallinity' and its quantification is a major contemporary concern in clay chemistry as reflected by the publication of the paper by Guggenheim *et al*. (2002) while the present manuscript was in preparation.

Similar concerns also extend to the study of bivalent layered hydroxides. Typical of this class of compounds is the mineral brucite, $Mg(OH)_2$, which comprises a hexagonal packing of hydroxyl ions, in which Mg^{2+} ions occupy alternate sheets of octahedral sites, resulting in a stacking of charge-neutral slabs having the composition $Mg(OH)_2$ (Oswald and Asper, 1977). Isostructural with this, but functionally far more useful is the hydroxide of Ni(II) known as β-nickel hydroxide. $Ni(OH)_2$ (space group, $P\bar{3}m1$; a = 3.12 Å, c = 4.6 Å) is the cathode material of all Ni-based alkaline secondary cells (McBreen, 1990). We have been interested for many years in the synthesis and characterization of $Ni(OH)_2$ and the correlation of its structure, composition and morphology with its electrochemical activity (Kamath *et al*., 1994; Dixit *et al*., 1999; Jayashree *et al*., 2000).

β-$Ni(OH)_2$ has interested solid-state chemists and battery technologists alike for a long time as its XRPD pattern shows variations which cannot be explained by the conventional arguments of Scherrer broadening. While various speculative explanations were offered in the early works on this subject (*e.g*. Barnard *et al*., 1981), the availability of modern computer codes such as DIFFaX (Treacy *et al*., 2000) has facilitated the classification as well as quantification of the extent of disorder in different preparations of a crystalline solid. The DIFFaX formalism considers a crystalline solid to comprise a stacking of planes of atoms and computes the XRPD pattern by integrating the diffraction intensities plane by plane (Treacy *et al*., 1991). Thus the DIFFaX

* E-mail address of corresponding author:
vishnu@sscu.iisc.ernet. in
DOI: 10.1346/CCMN.2003.0510511

Copyright © 2003, The Clay Minerals Society

https://doi.org/10.1346/CCMN.2003.0510511 Published online by Cambridge University Press

formalism is ideally suited for application to layered solids, where the layers naturally exist as an exigency of anisotropic bonding. DIFFaX has been used to analyze the nature of defects in graphite (Dittrich and Wohlfahrt-Mehrens, 2001), natural kaolinites (Artioli *et al.*, 1995), montmorillonite (Viani *et al.*, 2002) and $Li_{2/3}[Co_x Ni_{1/3-x}Mn_{2/3}]O_2$ (Lu and Dahn, 2001). Delmas and Tessier (1997) and Tessier *et al.* (1999) were the first to apply the DIFFaX formalism to β-$Ni(OH)_2$ and they succeeded in quantifying the various kinds of stacking faults in different preparations of this material. In an earlier work from this laboratory, DIFFaX was used to illustrate possible interstratification phenomena among the hydroxides of Ni(II) (Rajamathi *et al.*, 2000).

Several factors contribute to the deviation in the relative intensities and line-widths of different reflections from that expected of an ordered crystalline solid. We list below the possible factors:

(1) crystallite size measured in the (*a*-*b*) plane as the disc diameter and along the *c* axis as the thickness; (2) cation vacancies; (3) stacking faults; (4) turbostraticity; (5) interstratification; and (6) disorder in the intercalated species (the interlayer spacing (4.6 Å) in β-$Ni(OH)_2$ does not permit the inclusion of intercalated species and consequently this aspect is not relevant in the current discussion).

In this paper we investigate in a comprehensive way the specific effects of all these factors on the XRPD pattern of $Ni(OH)_2$. Since the conclusions of this study can be extended to other hexagonal layered solids, it is hoped that this paper will provide a rule of thumb to assist even the non-expert to deduce the nature of disorder in a hexagonal layered material by a mere inspection of the pattern of non-uniform broadening.

DIFFaX SIMULATIONS

The data used for DIFFaX simulations are described briefly here.

Layer description

The $Ni(OH)_2$ layer was modeled using the atomic position coordinates from the literature (Delmas and Tessier, 1997). The point group symmetry was declared to be unknown and all the symmetry-related atoms were completely described as: Ni (0, 0, 0); O1 (1/3, 2/3, 0.2060); O2 (−1/3, −2/3, −0.2060). Cation vacancies were simulated by specifying a fractional occupancy for the Ni site.

Crystal construction

The crystal is constructed by stacking the layers described one above another. Three identical layers were used for this purpose. To enable the stacking, a stacking vector is defined. The use of a single stacking vector (0, 0, 1) results in a perfectly ordered crystalline structure. The DIFFaX program was found to evaluate the point group symmetry around the Ni atom to be $-3m$, in keeping with our expectations.

Line width

The computed Bragg peaks are broadened by a Lorentzian function to simulate the effect of instrumental broadening. A line width of 0.3° is used since this corresponds to the sharpest observed line width in the experimental XRPD pattern of $Ni(OH)_2$.

Engineering disorder in the crystal

To engineer disorder in the crystal, different stacking vectors are employed. The probabilities with which the different stacking vectors are used are varied by hand until a satisfactory visual match between the observed and simulated patterns is obtained. The goodness of fit is judged by comparing the relative intensity and full width at half maximum (FWHM) value of each peak of the simulated pattern with that of the observed pattern. When these compare within limits of accuracy (±0.1°2θ) of the observed data, the best visual match is also obtained. The probabilities of the use of different stacking vectors then yield the relative abundance of the corresponding kinds of disorder.

Turbostratic disorder arising out of the random orientation of successive layers can be introduced in two ways: (1) by preserving the O–O distance between successive layers by the use of stacking vectors (1/3, 2/3, 1) and (2/3, 1/3, 1) along with (0, 0, 1). The use of these stacking vectors limits the angular orientation between the successive layers to $n \times 120°$. The use of the former two stacking vectors at low (<0.15) probabilities simulates the effect of stacking faults by the introduction of cubic ABC motifs in an otherwise hexagonal packing (Delmas and Tessier, 1997; Tessier *et al.*, 1999). The use of all three stacking vectors with equal (0.3333) probabilities yields a random packing of AB, CA, BC, AC..... layers, corresponding to turbostratic disorder. (2) By varying the O–O distance between successive layers by the use of a stacking vector $(x, y, 1)$ (x and y are random numbers) along with $(0, 0, 1)$. In this instance, the former permits any random angular orientation between successive layers. At low probabilities, $(x, y, 1)$ stacking has the same effect as that obtained by the introduction of stacking faults and at high probabilities this kind of stacking yields turbostratic disorder. We have verified that both methods yield the same result, when the diffraction intensity is computed for an infinite stacking.

The results presented in this paper are obtained by the second method as the use of the $(x, y, 1)$ stacking vector includes but is not limited to all manners of stacking faults, thus obviating the need to simulate the latter separately.

Interstratification is simulated by the use of the stacking vector $(x, y, 1.65)$. Such a stacking vector introduces motifs of a phase with an interplanar spacing

https://doi.org/10.1346/CCMN.2003.0510511 Published online by Cambridge University Press

of 7.6 Å (1.65×4.6 Å) within the host motifs of the β-phase (interplanar spacing = 4.6 Å). A polymorphic modification (α-phase) with an enhanced interplanar spacing (7.6 Å) has been reported among the hydroxides of Ni(II) (Oliva *et al.*, 1982). The increase in the interlayer distance is a consequence of hydration of the interlayer region.

EXPERIMENTAL

All $Ni(OH)_2$ samples were prepared by alkali-induced precipitation from $Ni(NO_3)_2$ solutions. The alkali and the precipitation conditions such as pH and temperature were varied to obtain precipitates of varying crystallinity. Sample A was prepared by adding ammonia (2 M, 100 mL) to $Ni(NO_3)_2$ (1 M, 50 mL) solutions (dropping rate = 5 mL/min.) at 65ºC and by ageing the slurry in mother liquor at 65ºC for a further 12 h period. Sample B was $Ni(OH)_2$ obtained from Aldrich Chemical Co. (USA) [Catalogue No. 283622]. Sample C was obtained by the addition of NaOH (2 M) to a solution of $Ni(NO_3)_2$ (1 M) at ambient temperature (26–28ºC) using a Metrohm Model 718 STAT titrino operated in the pH STAT mode. The addition of NaOH was stopped at a final pH = 9. Sample D was obtained at a constant high (>13) pH by the addition of $Ni(NO_3)_2$ (1 M, 50 mL) solution to NaOH (2 M, 100 mL) at 80ºC. All the samples were washed free of alkali and dried at 65ºC to constant weight.

All XRD patterns were obtained using a JEOL JDX8P powder X-ray diffractometer (CuKα source, λ = 1.541 Å). Wet chemical analysis of these samples was performed as described elsewhere (Dixit *et al.*, 1996).

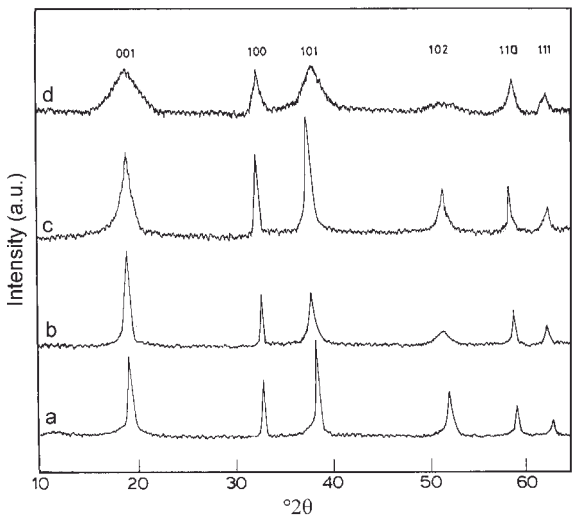


Figure 1. Observed XRPD patterns of β-$Ni(OH)_2$s: (a) sample A, (b) sample B; (c) sample C and (d) sample D.

RESULTS AND DISCUSSION

In Figure 1 typical XRPD patterns of $Ni(OH)_2$ samples obtained under different conditions are shown. While the Bragg peaks in the XRPD patterns of all samples appear at the expected positions (PDF: 14-117), the relative intensities and widths (measured as FWHM in 2θ) vary from sample to sample. Sample A is the most crystalline among those prepared. Except for the peaks due to 001 and 102 reflections (FWHM = 0.6º), all other peaks are equally broadened to a FWHM value of 0.3±0.1º2θ (see Figure 1a). In sample B, it is seen that the peaks corresponding to the *hk*0 reflections, *i.e.* 100 and 110, are much narrower than those due to the *h*0*l* (101 and 102) reflections (see Figure 1b). In sample C, there is further selective broadening of the 001 reflection (see Figure 1c). In sample D, the *hk*0 reflections are also broadened, in addition to the excessive broadening of the 001 and 101 reflections. The 102 reflection is broadened to the point of extinction (see Figure 1d). The widths of the various reflections in samples A–D are summarized in Table 1. We attribute these variations to different kinds of disorder. We examine below the effect of the inclusion of specific phenomena responsible for the broadening of the XRPD pattern of $Ni(OH)_2$.

Crystallite-size effects

Figure 2a shows the simulated XRPD pattern of the ideal structure with infinite crystallite size. Peak widths are defined purely on the basis of instrumental broadening, taken as Lorentzian with a FWHM = 0.3º2θ. As the thickness of the crystallites along the stacking direction of the layers is reduced (Figure 2b–c) broadening of the non-*hk*0 peaks is observed, the most affected peaks being those due to 001 and 102 reflections. The peaks due to the *hk*0 (100 and 110) reflections are unaffected. At a thickness of 37 layers (170 Å) (see Figure 2b), the FWHM of the 001 peak is 0.6º2θ, which is the typical value found in experimental patterns (samples A and B) for this reflection (Figure 1a,b). To achieve a broadening of the 001 reflection >1.5º (as in sample C), the thickness would have to be ~11 layers (50 Å). However, at a thickness of 17 layers (78 Å) (Figure 2c), additional peaks begin to emerge at low angles (10–20º) which grow rapidly in intensity (not shown) as the thickness is reduced below 17 layers. These low-angle reflections could either be

Table 1. The full width at half maxima (FWHM values in º2θ) of all the reflections in the XRPD patterns of the different β-$Ni(OH)_2$ samples.

Sample	001	100	101	102	110	111
A	0.6	0.3	0.4	0.6	0.4	0.6
B	0.6	0.3	0.9	broad	0.5	0.6
C	1.5	0.3	0.8	1.0	0.5	0.6
D	3.6	0.6	2.7	broad	0.5	1.4

https://doi.org/10.1346/CCMN.2003.0510511 Published online by Cambridge University Press

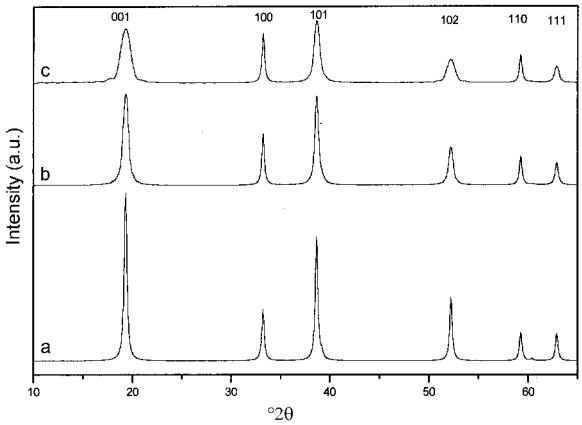


Figure 2. Simulated XRPD patterns of (a) crystalline β-$Ni(OH)_2$ with infinite thickness; (b) and (c) are the patterns obtained from simulations using thickness values of 37 and 17 layers, respectively.

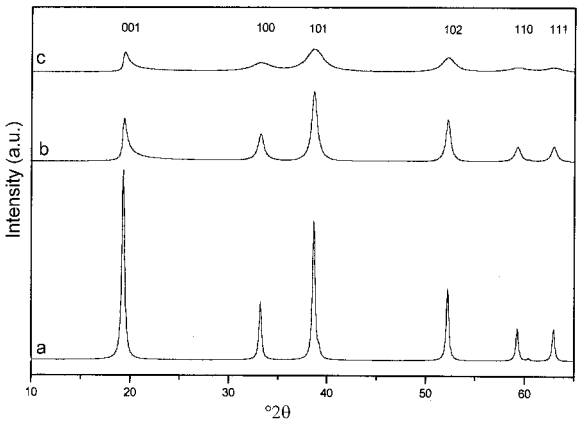


Figure 3. Simulated XRPD patterns of (a) crystalline β-$Ni(OH)_2$ with infinite disc diameter; (b) and (c) are the patterns obtained from simulations using disc diameters of 500 and 100 Å, respectively.

due to superstructures or due to oscillations in the Fourier transforms observed at thin crystal dimensions. Since such low-angle reflections are not observed in experimental patterns, we restrict the crystallite thickness to realistic values and conclude that broadening of the 001 peak beyond the FWHM value of 0.6° (as in samples C and D) cannot be ascribed purely to the crystallite thickness.

In Figure 3 the effect of disc diameter is shown. Any reduction in the disc diameter (below 1000 Å) leads to a broadening of the 100 reflection. As the observed patterns rarely exhibit broadening of the 100 peak (Figure 1), it is safe to ignore disc diameter as a determining factor in the non-uniform broadening of lines.

Cation vacancies

The DIFFaX simulations reported by Delmas *et al.* (1997, 1999) invariably overestimate the intensity of the 100 reflection when compared with the experimental pattern. The existence of Ni site vacancies in β-$Ni(OH)_2$ has been suggested by the neutron diffraction studies of Greaves and Thomas (1986) and independently confirmed by two groups (Bernard *et al.*, 1996; Cornilsen *et al.*, 1988, 1990) from Raman spectral studies. A structural model has been proposed which incorporates nearly 16% cation vacancies. These vacancies are compensated by the presence of protons at or near the octahedral vacancies. On the basis of these experimental results, a simulation of the XRPD pattern of $Ni(OH)_2$ containing Ni site vacancies was carried out (see Figure 4). On the inclusion of 20% Ni site vacancies, the relative intensity of the 100 reflection decreases by nearly 6%. This decrease in intensity occurs due to the overall reduction in the electron density at the cation sites.

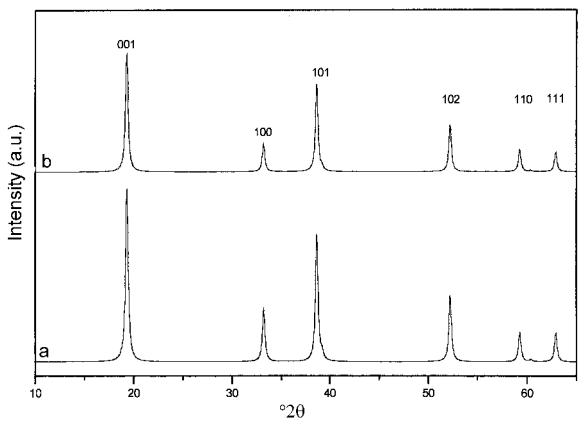


Figure 4. Simulated XRPD patterns of (a) crystalline β-$Ni(OH)_2$ and (b), (a) with 20% Ni site vacancies.

Stacking faults

Stacking faults are the most common type of disorder observed among layered solids. Barnard *et al.* (1981) ascribed the abnormal broadening of the *h*0*l* peaks in the XRPD pattern of β-$Ni(OH)_2$ to the presence of stacking faults. They correlated the electro-chemical activity of β-$Ni(OH)_2$ empirically to the line widths of the peaks due to the *h*0*l* reflections. Delmas and Tessier (1997) were the first to perform DIFFaX simulations to quantify the incidence of stacking faults in β-$Ni(OH)_2$. Their studies reveal that stacking faults cause the selective broadening of peaks due to the *h*0*l* (101 and 102) reflections.

Turbostraticity

The effects of the introduction of turbostraticity are shown in Figure 5. At low incidence, the effect of turbostraticity is the same as that of stacking faults studied by Delmas and Tessier (1997). The *h*0*l* reflections are broadened most; the 102 reflection is nearly extinguished at 15% incidence of turbostratic disorder

https://doi.org/10.1346/CCMN.2003.0510511 Published online by Cambridge University Press

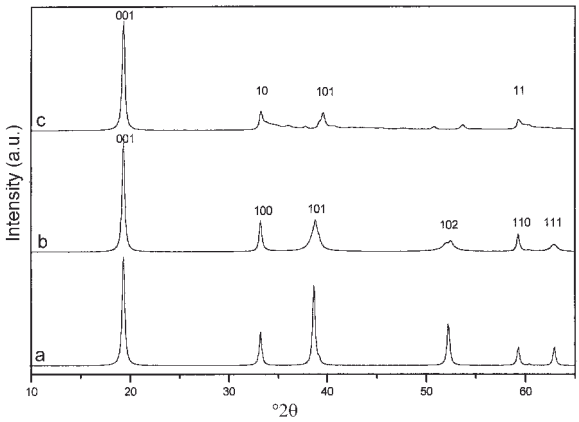


Figure 5. Simulated XRPD patterns of (a) crystalline β-Ni(OH)$_2$, (b), (a) with 15%, and (c), (a) with 80% turbostraticity, respectively.

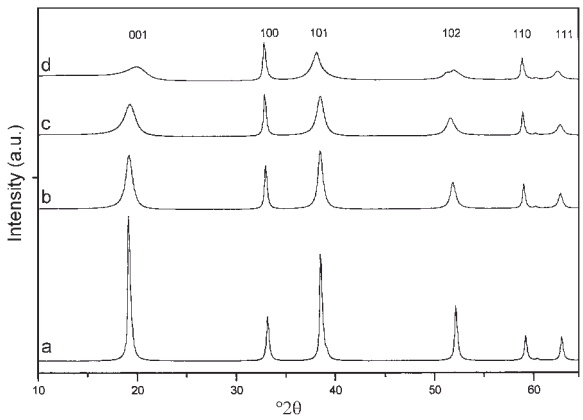


Figure 6. Simulated XRPD patterns of (a) crystalline β-Ni(OH)$_2$, (b) 5%, (c) 10% and (d) 25% of interstratified α motifs in β-Ni(OH)$_2$.

(see Figure 5b). At high (80%) incidence of turbostratic disorder, the *hk*0 reflections become essentially two-dimensional *hk*; and the 10 and 11 (formerly 100 and 110) reflections acquire a 'saw tooth' line shape, rising sharply and displaying an asymmetry on the higher-angle side (see Figure 5c). This feature has been predicted theoretically and observed experimentally for a host of layered materials including graphite and BN (Warren and Bodenstein, 1966; Andreev and Lundstrom, 1994). The width of the 00*l* reflection is unaffected by turbostratic disorder as the loss of registry between the layers does not affect the periodicity of the electron density function along the *c* crystallographic axis.

Interstratification

In Figure 6 the effect of interstratification of the β-Ni(OH)$_2$ with α motifs is shown. On the inclusion of even 5% α motifs, significant broadening of the 001, 101 and 102 reflections is seen (Figure 6b). On further increase of the incidence of α motifs to the 10–25% range (see Figure 6c–d), progressive broadening of these reflections is seen with near extinction of the intensities of the 001, 102 and 111 reflections at 25% interstratification. The 100 and 110 reflections remain essentially unchanged compared to the pattern of the crystalline sample. Interstratification appears to broaden all the non-*hk*0 reflections.

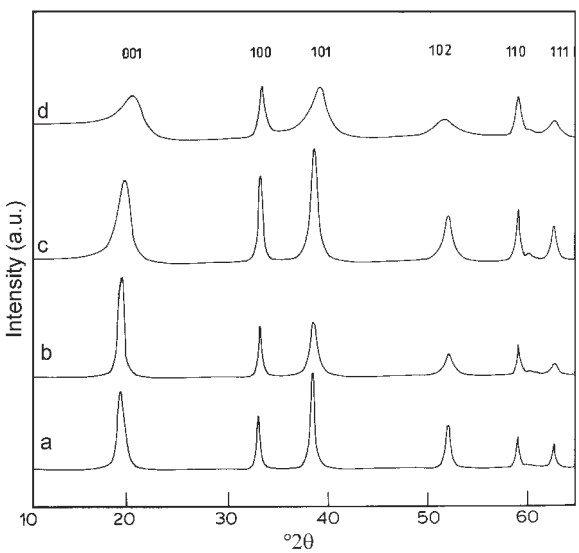


Figure 7. Results of simulations of the experimental patterns, (a) sample A, (b) sample B, (c) sample C, (d) sample D.

Simulation of the experimental patterns

The simulation of the experimental patterns is shown in Figure 7. The XRPD pattern of sample A could be simulated exclusively on the basis of crystallite size (disc diameter, 10,000 Å; thickness, 207 Å) (see Figure 7a). The XRPD pattern of sample B was simulated by a combination of crystallite size (disc diameter, 11,500 Å; thickness, 184 Å) and turbostraticity (14%) (see Figure 7b). The XRPD pattern of sample C could be simulated by the inclusion of interstratification (10%) while sample D is a combination of interstratification (23%), turbostraticity (10%) and cation vacancies (17%) (Figure 7c–d). These results are summarized in Table 2. As in any fitting procedure, the solutions arrived at may not be unique. Different solutions vary slightly in the quantification of disorders, but invariably agree in the prediction of specific disorders. This agreement, we believe, is significant and gives an insight into the nature of the material.

CONCLUSIONS

DIFFaX simulations suggest that stacking faults broaden *h*0*l* reflections while turbostraticity causes the asymmetric broadening of the *hk*0 reflections. Interstratification broadens all the non-*hk*0 reflections. From an examination of the pattern of non-uniform

https://doi.org/10.1346/CCMN.2003.0510511 Published online by Cambridge University Press

Table 2. Results of DIFFaX simulations of the XRPD patterns of $Ni(OH)_2$.

Preparative method	Sample	Crystallite size (Å) Thickness	Disc diameter	Cation vacancies (%)	Turbostraticity (%)	Interstratification (%)
Ammonia-induced precipitation	A	207	10,000	–	–	–
Aldrich Chemical Co. (USA)	B	184	11,500	–	14	–
Strong alkali-induced precipitation (pH = 9)	C	–	–	–	–	10
Strong alkali-induced precipitation (pH >13)	D	–	–	17	10	23

broadening, it is possible to characterize the nature of disorder in hexagonal layered solids.

ACKNOWLEDGMENTS

The authors thank the Department of Science and Technology, Government of India (GOI) for financial support. TNR and RSJ thank the Council of Scientific and Industrial Research, GOI, for the award of Junior Research (NET) and Senior Research (NET) Fellowships, respectively.

REFERENCES

Andreev, Y.G. and Lundstrom, T. (1994) In-plane lattice-parameter and crystallite-size determination in a turbostratic graphite-like structure. *Journal of Applied Crystallography*, **27**, 767–771.

Artioli, G., Bellotto, M., Gualtieri, A. and Pavese, A. (1995) Nature of structural disorder in natural kaolinites: A new model based on computer simulation of powder diffraction data and electrostatic energy calculation. *Clays and Clay Minerals*, **43**, 438–445.

Barnard, R., Randell, C.F. and Tye, F.L. (1981) Studies concerning the ageing of α and β-$Ni(OH)_2$ in relation to nickel-cadmium cells. Pp. 401–425 in: *Power Sources*, vol. **8**. Academic Press London.

Bernard, M.C., Cortes, R., Keddam, M., Takenouti, H., Bernard, P. and Senyarich, S. (1996) Structural defects and electrochemical reactivity of β-$Ni(OH)_2$. *Journal of Power Sources*, **63**, 247–254.

Cornilsen, B.C., Karjala, P.J. and Loyselle, P.L. (1988) Structural models for nickel hydroxide electrode active mass. *Journal of Power Sources*, **22**, 351–357.

Cornilsen, B.C., Shan, X. and Loyselle, L. (1990) Structural comparison of nickel electrodes and precursor phases. *Journal of Power Sources*, **29**, 453–456.

Delmas, C. and Tessier, C. (1997) Stacking faults in the structure of nickel hydroxide: a rationale of its high electrochemical activity. *Journal of Materials Chemistry*, **7**, 1439–1443.

Dittrich, H. and Wohlfahrt-Mehrens, M. (2001) Stacking fault analysis in layered materials. *International Journal of Inorganic Materials*, **3**, 1137–1142.

Dixit, M., Subbanna G.N. and Kamath, P.V. (1996) Homogeneous precipitation from solution by urea hydrolysis: a novel chemical route to the α-hydroxides of nickel and cobalt. *Journal of Materials Chemistry*, **6**, 1429–1432.

Dixit, M., Kamath, P.V. and Gopalkrishnan, J. (1999) Zinc-substituted α-Nickel hydroxide as an electrode material for alkaline secondary cells. *Journal of the Electrochemical Society*, **146**, 79–82.

Greaves, C. and Thomas, M.A. (1986) Refinement of the structure of deuterated nickel hydroxide, $Ni(OD)_2$, by powder neutron diffraction and evidence for structural disorder in samples with high surface area. *Acta Crystallographica*, **B42**, 51–55.

Guggenheim, S., Bain, D.C., Bergaya., F., Brigatti, M.F., Drits, V.A., Eberl, D.D., Formoso, M.L.L., Galán, E., Merriman, R.J., Peacor, D.R., Stanjek, H. and Watanabe, T. (2002) Report of the Association Internationale pour l'Etude des Argiles (AIPEA) nomenclature committe for 2001: order, disorder and crystallinity in phyllosilicates and the use of the 'crystallinity index'. *Clays and Clay Minerals*, **50**, 406–409.

Jayashree, R.S., Kamath, P.V. and Subbanna, G.N. (2000) The effect of crystallinity on the reversible discharge capacity of nickel hydroxide. *Journal of the Electrochemical Society*, **147**, 2029–2032.

Kamath, P.V., Dixit, M., Indira, L., Shukla, A.K., Ganesh Kumar, V. and Munichandraiah, N. (1994) Stabilized α-$Ni(OH)_2$ as electrode material for alkaline secondary cells. *Journal of the Electrochemical Society*, **141**, 2956–2959.

Lu, Z. and Dahn, J.R. (2001) Effects of stacking fault defects on the X-ray diffraction patterns of T2, O2, and O6 structure $Li_{2/3}[Co_xNi_{1/3-x}Mn_{2/3}]O_2$. *Chemistry of Materials*, **13**, 2078– 2083.

McBreen, J. (1990) The nickel oxide electrodes. Pp. 28–63 in: *Modern Aspects of Electrochemistry*, vol. **21** (R.E. White, J.O'M. Bockris and B.E. Conway, editors). Plenum Press, New York.

Oliva, P., Leonardi, J., Laurent, J.F., Delmas, C., Braconnier, J.J., Figlarz, M., Fievet, F. and Guibert, A. de (1982) Review of the structure and the electrochemistry of nickel hydroxides and oxy-hydroxides. *Journal of Power Sources*, **8**, 229–255.

Oswald, H.R. and Asper, R. (1977) Bivalent metal hydroxides. Pp. 71–140 in: *Preparation and Crystal Growth of Materials with Layered Structures*, vol. **1** (R.M.A. Lieth, editor). Reidel Publishing Company, Dordrecht, The Netherlands.

Rajamathi, M., Kamath, P.V. and Seshadri, R. (2000) Polymorphism in nickel hydroxide: role of interstratification. *Journal of Materials Chemistry*, **10**, 503–506.

Tessier, C., Haumesser, P.H., Bernard, P. and Delmas, C. (1999) The structure of $Ni(OH)_2$: From the ideal material to the electrochemically active one. *Journal of the Electrochemical Society*, **146**, 2059.

Treacy, M.M.J., Deem, M.W. and Newsam, J.M. (2000) *Computer code DIFFaX,* Version 1.807.

https://doi.org/10.1346/CCMN.2003.0510511 Published online by Cambridge University Press

Treacy, M.M.J., Newsam, J.M. and Deem, M.W. (1991) A general recursion method for calculating diffracted intensities from crystals containing planar faults. *Proceedings of the Royal Society, London*, **A433**, 499–520.

Viani, A., Gualtieri, A.F. and Artioli, G. (2002) The nature of disorder in montmorillonite by simulation of X-ray powder patterns. *American Mineralogist*, **87**, 966–975.

Warren, B.E. and Bodenstein, P. (1966) The shape of two-dimensional carbon black reflections. *Acta Crystallographica*, **20**, 602–605.

West, A.R. (1987) *Solid State Chemistry and its Applications*. John Wiley and Sons, Singapore.

(*Received 1 November 2002; revised 23 April 2003; Ms. 734; Peter J. Heaney*)

https://doi.org/10.1346/CCMN.2003.0510511 Published online by Cambridge University Press